Supporting Information for:

Hybrid Heterojunctions of Solution-Processed Semiconducting 2D Transition Metal Dichalcogenides

Xiaoyun Yu[1], Aiman Rahmanudin[1], Xavier A. Jeanbourquin[1], Demetra Tsokkou[2], Néstor Guijarro[1], Natalie Banerji[2] and Kevin Sivula[1]*

1) Laboratory for Molecular Engineering of Optoelectronic Nanomaterials, École Polytechnique Fédérale de Lausanne (EPFL), Station 6, 1015 Lausanne, Switzerland.

2) Department of Chemistry, University of Fribourg, Chemin du Musée 9, CH-1700 Fribourg, Switzerland

*Email: kevin.sivula@epfl.ch

S1. TMD electrode preparation and characterization

Exfoliation: Commercially available TMD powder was exfoliated by solvent assisted exfoliation method. Typically, 0.5 g MoS_2 powder (Aldrich, 99%, <2 μm) was dispersed in 50 mL NMP and sonicated by Qsonica Q700 probe sonicator (50% amplitude, 10 s / 2 s duty cycle) for 6 h in 0 °C bath. After sonication, dispersion was centrifuged at 1500 rpm for 60 min to remove unexfoliated particles. Then soluble impurities were removed from the dispersion by centrifugation (7500 rpm, 30 min). Precipitated MoS_2 flakes were re-dispersed in 25 mL NMP for thin film formation. For

MoSe$_2$ (Alfa Aesar, 99.9% -325 mesh powder) exfoliation, a similar process was used except for longer sonication time (12h).

SCSA film deposition: TMD thin films were deposited by a modified space-confined self-assembly method[S1] to tolerate TMD flakes exfoliated in N-methyl-2-pyrrolidone (NMP) without additional additives to stabilize the dispersion. Specifically, F-doped SnO$_2$ (FTO) coated substrates (size 3×3 cm^2) were placed in a fritted funnel which was filled by two immiscible solvents to create a liquid-liquid interface (area of 16 cm^2). In the case of assembly from NMP dispersions, hexane (ca. 10 mL) was used as the top phase and water:acetonitrile (85:15, v/v, ca. 15 mL) as the bottom phase. The exfoliated TMD dispersion (0.5-1 mg mL^{-1}) was injected using a syringe to the interface continuously until a compact film is formed at the interface. Generally ca. 10 µL of the TMD dispersion is used per 1 cm^2 of liquid-liquid interface, consistent with one layer of TMD flakes at the liquid-liquid interface with average thickness of ca. 10 nm. The top liquid phase was removed and dried by air flow then the bottom phase was removed by vacuum assisted filtration to allow the thin films at the interface to deposit on the substrates. Thin films deposited on the FTO substrates were allowed to dry naturally, followed by heating in N$_2$ at 250 ℃ for 30 min to remove all adsorbed solvent.

DHA-PDI overlayer coating: For DHA-PDI deposition, 5 mg DHA-PDI powder (synthetic route described see the following section S2) was dispersed in 1 mL H$_2$O:isopropanol (1:1 v/v) solvent. 5 µL 2 M KOH was added to assist solubility. This solution was spin-coated at 1500 rpm for 30 s followed by 3000 rpm for 2 s. After drying at 100 ℃ for 10 min, the films were immersed into 1 M HCl in water:ethanol (1:2, v/v) to neutralize the DHA-PDI. All films were annealed in the air at 200 ℃ for 20 min before photoelectrochemical measurements.

Deposition of KPFM sample: A DHA-PDI layer with thickness of ca. 50 nm was first coated on a glass substrate, in such a way to leave parts of the bare glass exposed after being neutralized in HCl solution. Then a sparsely packed MoS_2 film was deposited on the glass/DHA-PDI.

Characterization: The morphology of thin films was observed by SEM (Zeiss Merlin) and TEM (FEI Tecnai Osiris) electron microscopes. UV-vis absorption spectra were recorded by Shimadzu UV-vis-NIR UV-3600 spectrophotometer using integral sphere. Reflected light and baseline beyond 850 nm was subtracted to obtain absorption spectrum. Surface potential (KPFM) images were obtained by Cypher atomic force microscope (Asylum Research).

Photoelectrochemical measurements: experiments were carried out using a BioLogic SP-200 potentiostat in a three-electrode configuration using a Capuccino-type cell. A Pt wire and Ag/Ag^+ non-aqueous electrode were used as counter electrode and reference, respectively. The geometric area for the working electrode was 0.25 cm^2. The electrolyte contains 25 mM LiI (99.9 %, Aldrich) in 0.1 M tetrabutylammonium perchlorate (TBAP) acetonitrile solution. Illumination was performed with a 500 W Muller Electronik Xenon-arc lamp coupled to a KG-1 filter (Schott), calibrated to 1 sun (AM 1.5G, 100 mW cm^{-2}) irradiance. Linear sweep voltammetry was performed at a scan rate of 10 mV s^{-1}. Incident photon to current efficiencies (IPCE) was obtained using a Tunable PowerArc illuminator (Optical Building Blocks Corporation). The photon flux was calibrated with a S120VC Photodiode Power Sensor (Thorlabs). Working electrodes were illuminated from the substrate side in all cases.

S2. Synthetic procedures for PDI derivatives

Synthetic methods and characterization: All reagents were of commercial reagent grade (Sigma-Aldrich, Acros and Fluorochem) and were used without further purification. Solvents chloroform (Fisher Chemical, HPLC grade) and DMSO (Sigma-Aldrich, Reagent Grade) were used

without further purification. Normal phase silica gel chromatography was performed with an Acros Organic silicon dioxide (pore size 60 Å, 40–50 μm technical grades) and reverse phase silica gel chromatography was performed with a Material Harvest C18 reverse phase silica gel (pore size 60 Å, 40-63 μm). The (^{1}H) and (^{13}C) NMR spectra were recorded at room temperature using per-deuterated solvents as internal standards on a NMR Bruker Advance III-400 spectrometer (Bruker, Rheinstetten, Germany). Chemical shifts are given in parts per million (ppm) referenced to residual ^{1}H or ^{13}C signals in CDCl$_3$ and DMF-d_7 (1H: 7.26, 13C: 77.0). Mass spectrometry measurements were performed on a MALDI-TOF AutoFlex speed with a Smartbeam^{TM}-II 2 kHz laser from Bruker. Fourier transform infrared spectroscopy (FTIR) spectra were recorded on a FTS 7000(e) Series from Portman Instruments AG (Biel-Benken, Germany). Synthesis of PDI derivatives were based on modified from literature procedures as indicated below.

Synthesis of PDI dicarboxylic acids
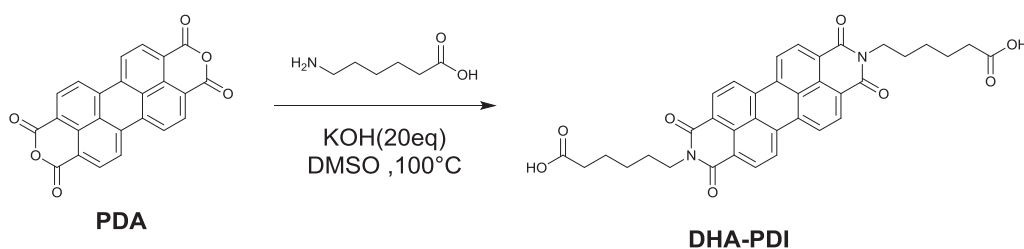
Scheme S1. Procedure for (C$_5$COOH)$_2$PDI (from Rehm, Stepanenko et al. 2010, ref S2)

Perylene-3,4,9,10-tetracarboxylicdianhydride **PDA** (1.0g, 2.55mmol) was suspended in DMSO (100 mL) and heated to 100 °C for 30mins. 6-aminocaprioc acid (6.69g, 50.9 mmol) and KOH (2.86g, 50.9 mmol) was then dissolved in water and added into the reaction mixture slowly. The mixture was stirred for 3 h at 100 °C, cooled down to room temperature. Subsequently, adjusting mixture to pH 5 with aqueous hydrochloric acid. The precipitate was centrifuged several times, with water (2 × 50 mL) and methanol (2 × 50 mL). The red solid was then boiled in 2 M HCl (100 mL) and the solution was filtrated hotly. The residue was then washed with hot 2 M HCl (50 mL) and

water (50 mL) several times, and afterwards the red solid was dried under vacuum overnight to obtain **DHA-PDI** as a dark red solid (1.428g, 90.6%).

^{1}H NMR (400 MHz, DMF-d_7) δ 9.17 (d, J = 8.2 Hz, 4H), 8.80 (d, J = 8.0 Hz, 4H), 4.375-4.343 (m, 4H), 2.54 (t, J = 7.5 Hz, 4H), 1.99-1.962 (m, 4H), 1.90-1.87 (s, 4H), 1.726-1.684 (m, 4H); FT-IR(KBr): 3475-2736(b), 2952(s), 2937(s), 1265(s), 1341(s), 1594(s)1652(s), 169.3(s),); MS(MALDI-TOF) (*m/z*): $C_{36}H_{30}N_2O_8$, 620.27[M+2H]$^+$, Calcd: 618.20; m.p: 210 °C.

The following FTIR spectrum of DHA-PDI clearly shows the –COOH, –CH and –CH signals at 2500-3500 cm^{-1} indicating the success functionalization of the PDI molecule with carboxylic acid group, while the peaks below 2000 cm^{-1} are consistent with the PDI core fingerprint spectra.[S2]
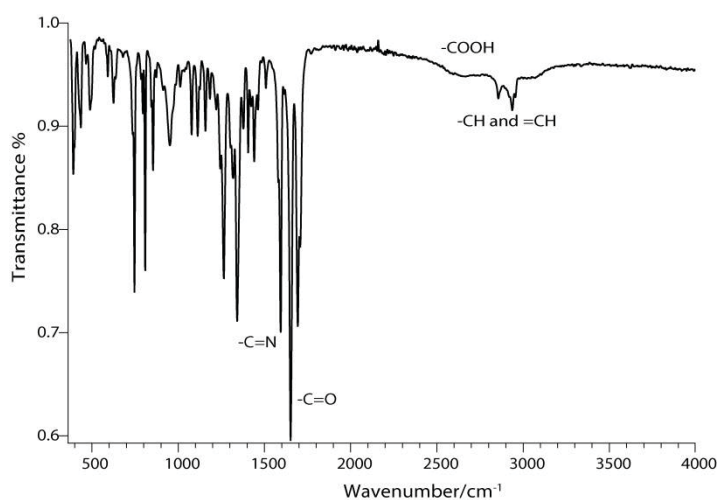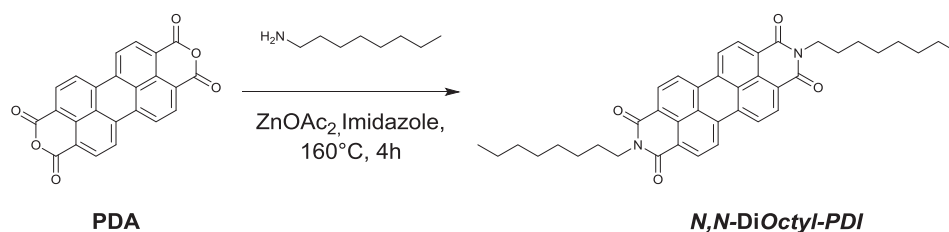

Figure S0. FTIR spectrum for DHA-PDI powder

Synthesis of symetric alkylation of PDA

PDA

N,N-Di*Octyl*-PDI

Scheme S2. Procedure for N,N-dioctyl PDI (from Savage, Orgiu et al. 2012 Ref S3)

Perylene-3,4,9,10-tetracarboxylicdianhydride PDA (1.0g, 8.94mmol), Zn(OAc)$_2$ (0.320g, 1.91 mmol), imidazole (5.0 g) and n-octylamine(0.988g, 7.65mmol) was vigorously stirred at 160 °C for 2 h. After cooling to r.t., the mixture was dissolved in minimum amount of THF and precipitated in 300 mL 2N HCl/MeOH 2:1 V/V. The precipitate was collected by filtration, washed with H$_2$O followed by MeOH and dried at 80 °C in vacuum. The crude product was further purified by column chromatography using chloroform as eluent to obtain *N,N*-DiOctyl-PDI as a reddish-brown solid (76.6%, 1.95mmol). ^{1}H NMR (400 MHz, Chloroform-*d*) δ 8.70 (d, *J* = 8.0 Hz, 4H), 8.63 (d, *J* = 8.1 Hz, 4H), 4.21 (t, *J* = 7.8 Hz, 4H), 1.76 (q, *J* = 7.9 Hz, 4H), 1.41 (d, *J* = 101.7 Hz, 10H), 0.87 (q, *J* = 11.0, 8.3 Hz, 6H).; MS: 615.539 (MALDI-TOF); Calcd. [C$_{40}$H$_{42}$N$_2$O$_4$]: 614.31.

S3. Thin film morphology characterization

TMD flakes were exfoliated in N-methyl-2-pyrrolidone (NMP) without additional additives to stabilize the dispersion. A wide field-of-view top-down scanning electron micrograph (SEM) in Figure S1 shows the resulting film of 2D MoS$_2$ flakes on FTO-glass substrates, and Figure S2a shows the same film with a narrow field view. The 2D flakes range in lateral dimension from ca. 100 nm to over 500 nm, consist of a few atomic layers, and form an optically homogeneous layer (free from aggregation) where the flakes are aligned parallel with the substrate surface.

For the organic semiconductor, we found that the solution processing of N,N-dioctyl PDI in organic solvents favored the aggregation and pi-stacking of the PDI with itself and limited the coverage of the MoS$_2$ film due to poor wetting characteristics as shown in Figure S3. However, processing N,N-dihexanoic acid functionalized in aqueous solution by spin coating gave homogeneous films of PDI both on bare FTO and on the self-assembled MoS$_2$ nanoflake films (see optical images of large-area electrodes in the main text). Overall it is important to point out that our

mild solution-based deposition procedure is suitable for a variety of substrates including bare SiO_2 and flexible Sn-doped In_2O_3 (ITO) on plastic.

A top-down SEM image of the MoS_2/DHA-PDI bilayer hybrid film (Figure S2b) shows a similar morphology to the bare MoS_2 film consistent with the presence of a thin homogeneous film of the organic semiconductor. Careful comparison of the SEM images in Figure S2 before and after DHA-PDI deposition suggest a rougher flake surface in the hybrid film compared to the bare MoS_2. A high-resolution cross-sectional SEM image of a single flake (Figure S4) indicates that organic material was deposited on both the surface and edges of the 2D flake. This homogeneous coverage implies the non-covalent bonding of DHA-PDI on MoS_2 and indicates that a possible preferential affinity of the carboxylic acid functionality to exposed Mo atoms at flake edges was not a principal mechanism for the deposition. However, we cannot discount the presence of the DHA-PDI at these sites. Direct measurement of the thickness of the DHA-PDI layer on the MoS_2 was difficult due to the ultrathin coating and relative large roughness of the surface, however the cross-sectional SEM image (Figure S4) suggests the thickness is in the range of 10 nm.
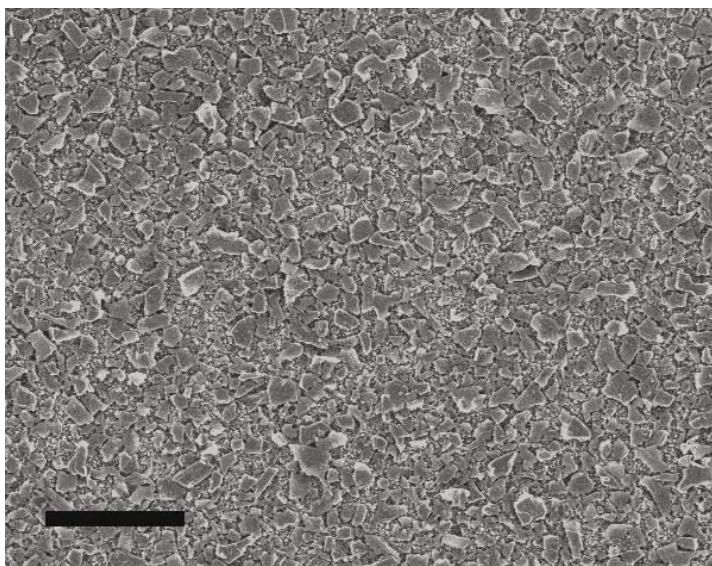

Figure S1. SEM image of MoS_2 thin film deposited on FTO glass by space confined self-assembly method (scale bar is 2 μm).
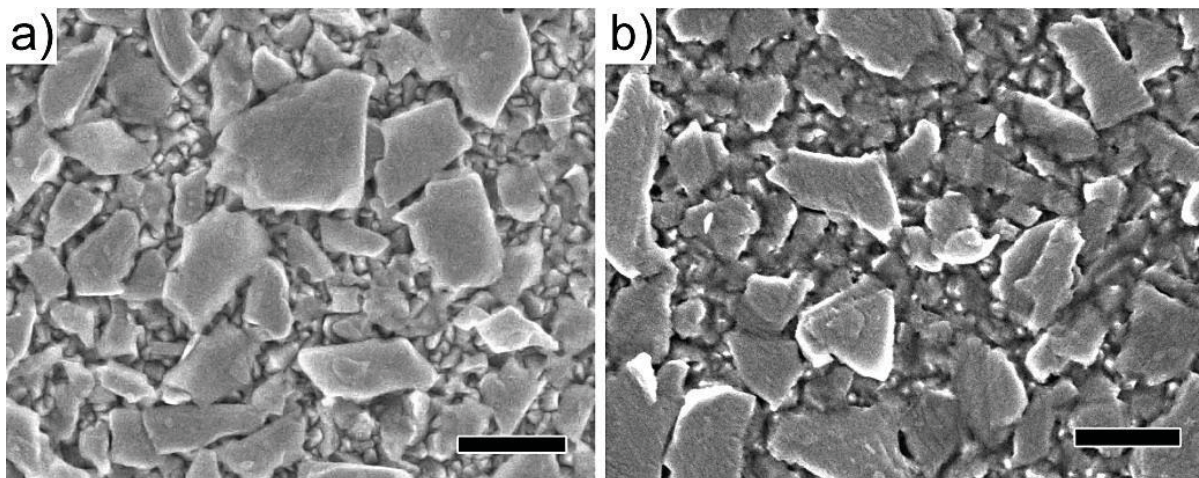
Figure S2. Top-down SEM image of (a) a MoS$_2$ thin film deposited on FTO glass by the liquid-liquid self-assembly technique, and (b) a N,N-dihexanoic acid functionalized PDI coated MoS$_2$ films. The scale bars are 500 nm in both images.
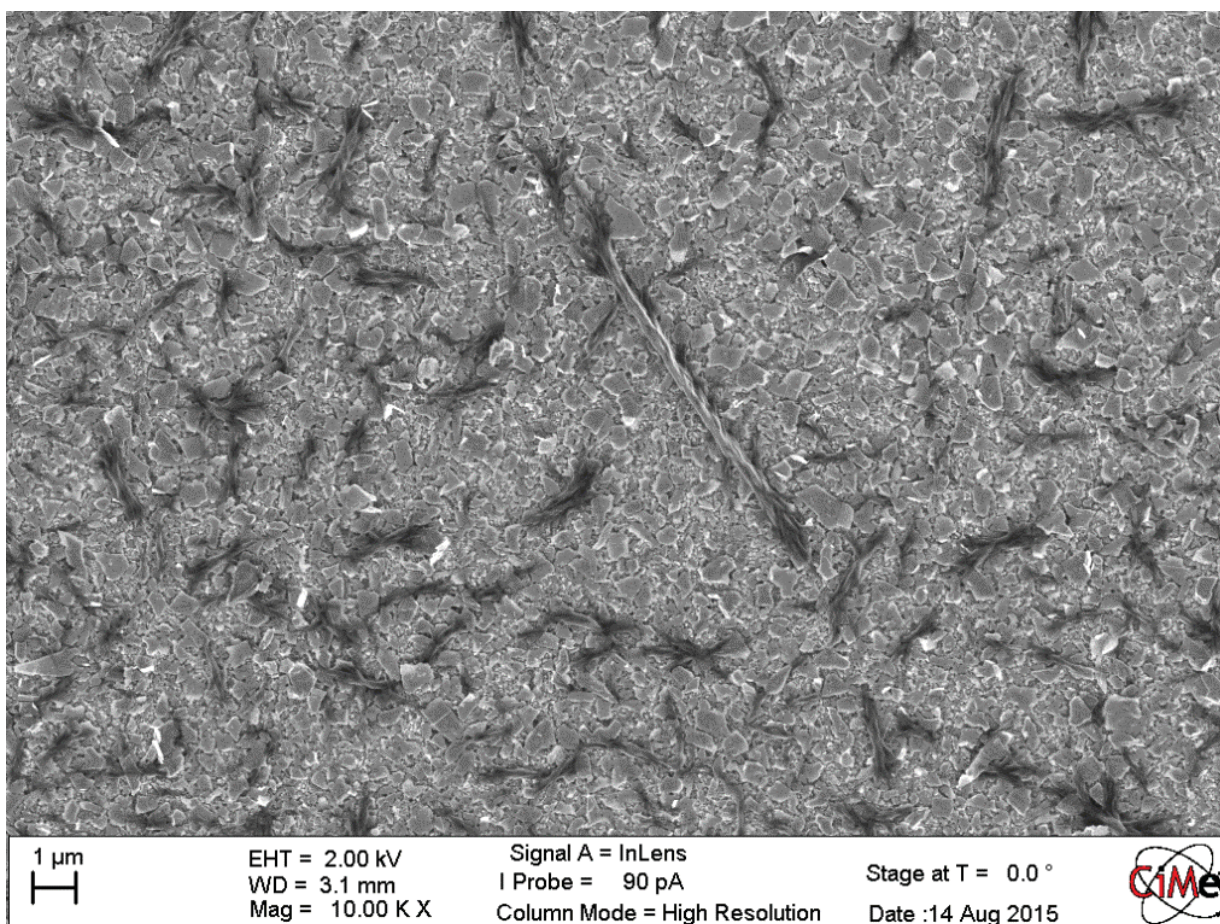

1 µm	EHT = 2.00 kV	Signal A = InLens	Stage at T = 0.0°
	WD = 3.1 mm	I Probe = 90 pA	
	Mag = 10.00 K X	Column Mode = High Resolution	Date :14 Aug 2015

Figure S3. SEM image of MoS$_2$/N,N-dioctyl-perylene-diimide hybrid film shows exposed MoS$_2$ and large PDI fibers.
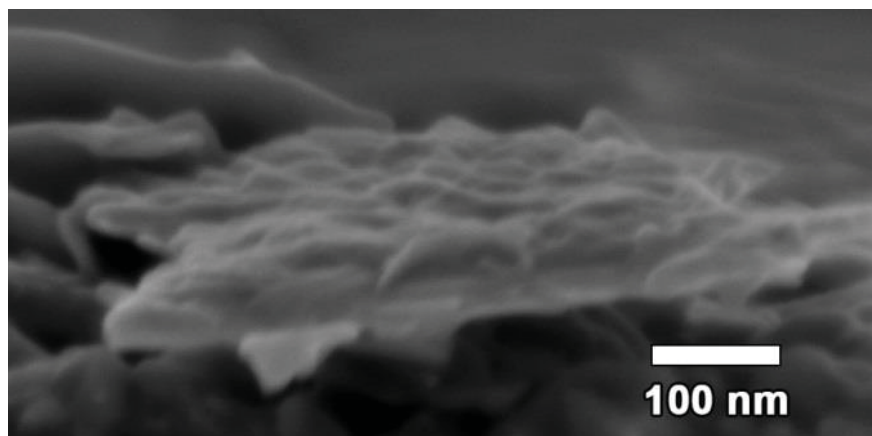
Figure S4. a cross-sectional SEM image of a single MoS_2 flake with DHA-PDI coating

S4. Other Additional Figures
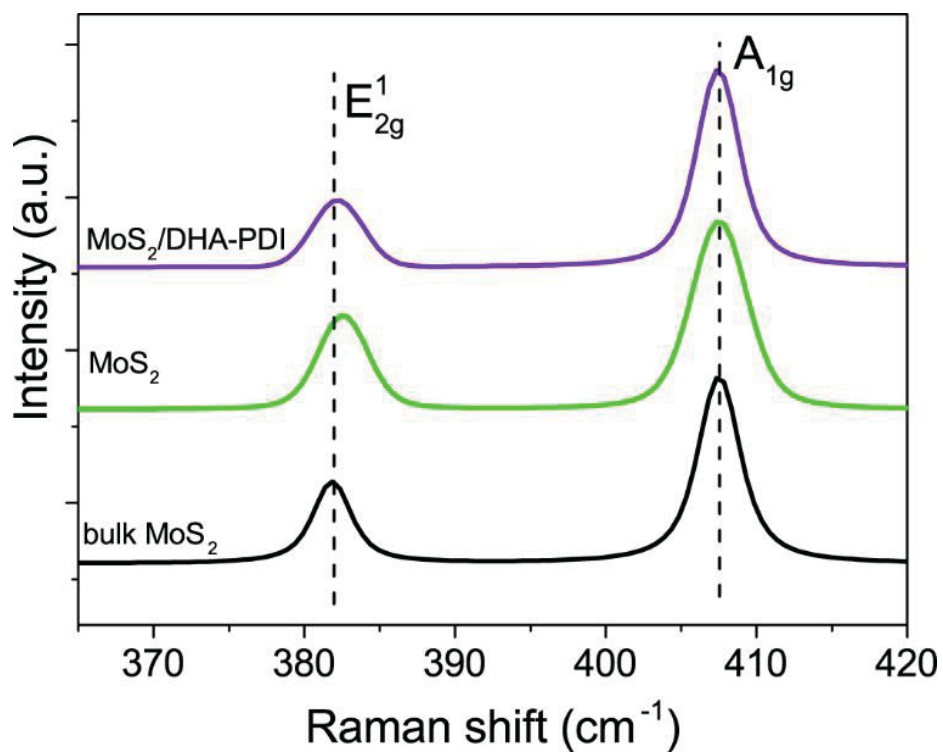
Figure S5. Raman spectra of bulk MoS_2 powder and MoS_2 in bare and MoS_2/DHA-PDI hybrid films deposited on FTO substrates.
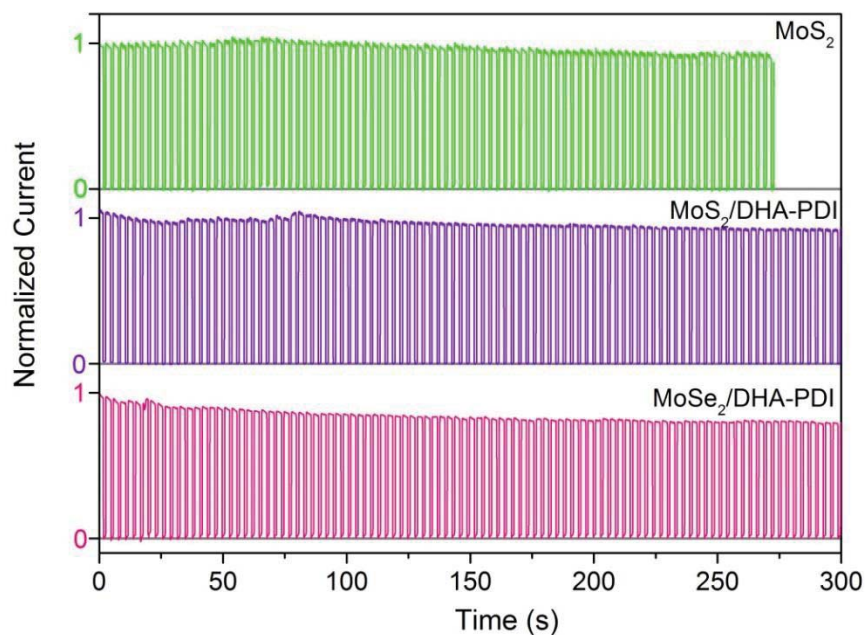
Figure S6. Chronoamperometric measurements of MoS_2, MoS_2/DHA-PDI and $MoSe_2$/DHA-PDI hybrid electrodes with I^-/I_3^- redox couple under intermittent illumination at $+0.1$ V vs Ag/Ag$^+$. For MoS_2/DHA-PDI electrode, ca. 0.12 C current (1.25 μmol electrons) passed through the active area during the scan, while material loading on electrode is estimated to be ca. 0.5 nmol for PDI molecules and ca. 8 nmol for MoS_2.
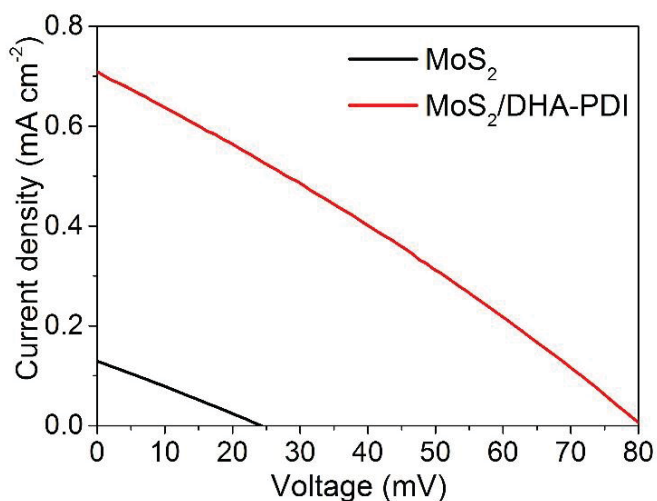

Figure S7. J-V curves of the two electrode liquid junction sandwiched photovoltaic cells based on MoS_2 and MoS_2/DHA-PDI photoanodes. Pt-coated FTO counter electrode and acetonitrile iodide/poly-iodide (0.1 M LiI + 0.01 M I$_2$) electrolyte were used, with active area of 0.19 cm^2.
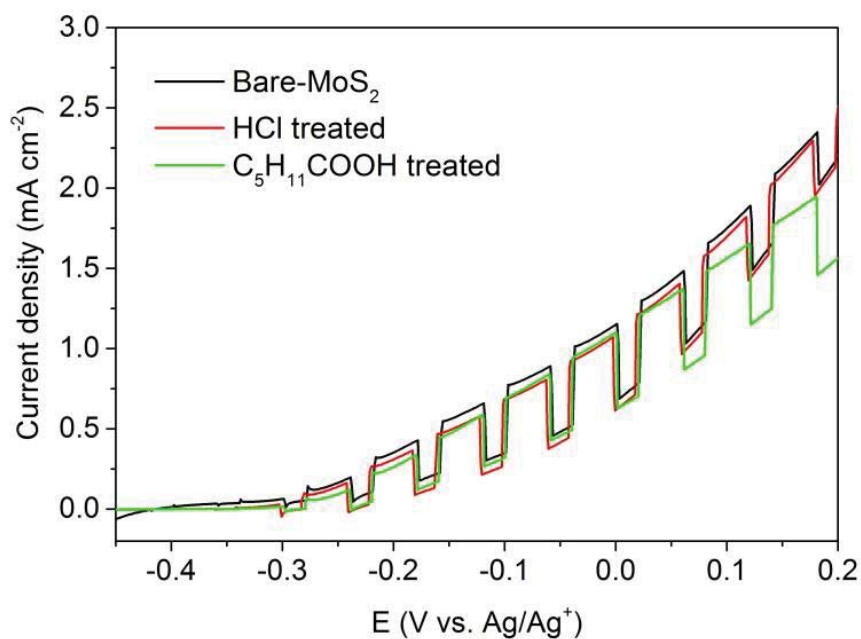
Figure S8. Control experiments: J-V curves of the MoS$_2$ films exposed to hexanoic acid or HCl solution show no obvious improvement compared to MoS$_2$ bare electrode. The decreased dark current and slightly increased photocurrent of the hexanoic acid treated electrode can be attributed to the passivation of exposed substrate by hexanoic acid.
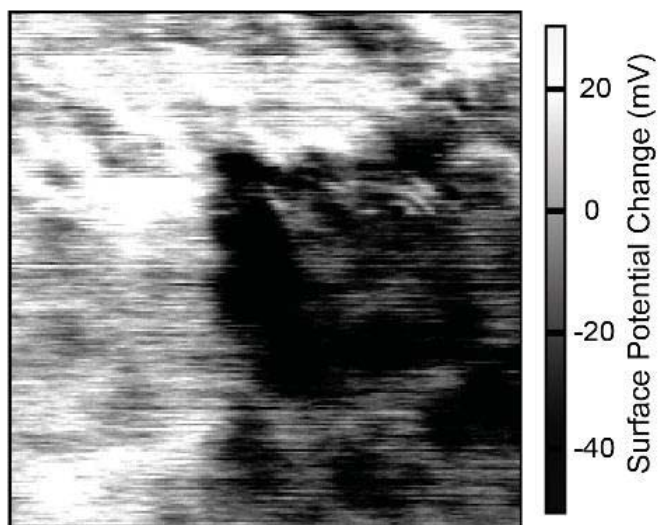

Figure S9. Map of the surface potential difference (light minus dark) calculated from the KPFM surface maps shown in Figure 2 (main text).
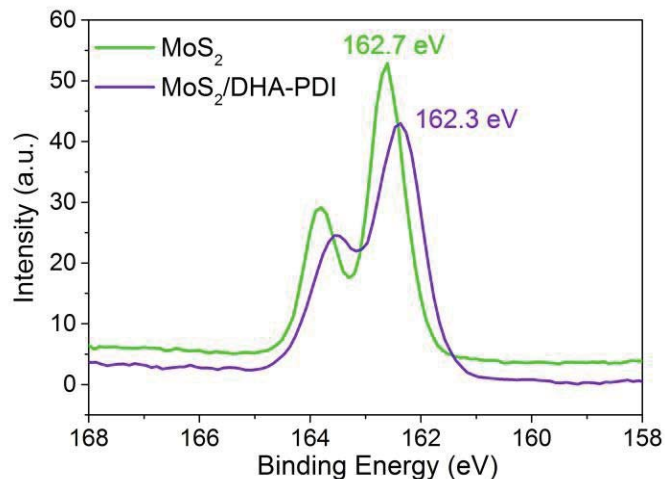
Figure S10. XPS S 2p spectra of the MoS_2 and MoS_2/DHA-PDI hybrid thin films. The hybrid film shows a 0.4 eV red-shift after DHA-PDI deposition, consistent with the Mo core level and valence band shift as described in the main text.
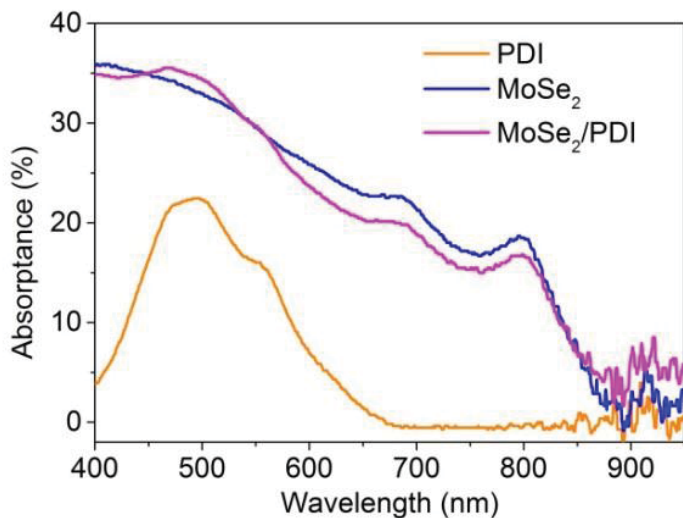

Figure S11. UV-vis absorptance spectra of $MoSe_2$ and $MoSe_2$/DHA-PDI films.
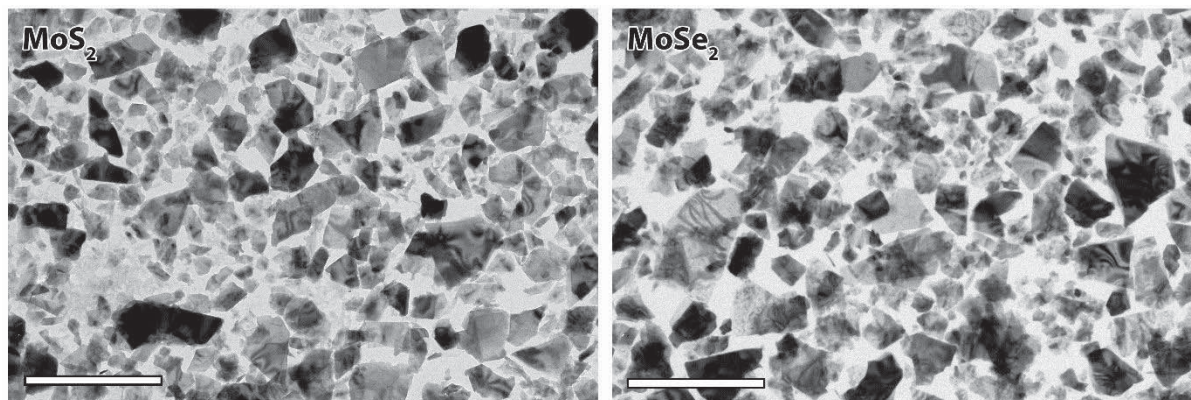

Figure S12. TEM images of solvent exfoliated MoS_2 (left) and $MoSe_2$ (right) flakes used in this work. The scale bars are 1 μm in both images.

S5. Transient absorption measurement

Method

Transient absorption (TA) measurements were performed using excitation pulses at 600 nm generated from the fundamental near-infrared pulses (30 fs, 800 nm, 1 kHz, 6 mJ, Astrella Coherent) and frequency-converted in an optical parametric amplifier (OPA, Opera Solo, Coherent). Broadband white light probe pulses covering the visible region from 450 nm to 750 nm were generated in a sapphire plate using a part of the fundamental beam. The white light was split into two components that serve as the signal and reference pulses. The probe pulses were temporally delayed relative to the excitation pulses via a micrometer translation stage, and pump-probe delays up to 1 ns were measured. Pump pulses of ~ 1 mm diameter photo-excited the sample (chopped at half the laser frequency), while the weaker probe pulses of ~ 250 μm diameter were used to probe the changes induced by pump excitation at different pump-probe delays. The different pump and probe beam diameters ensured a uniform distribution of detected photo-excited species. The signal probe pulses transmitted through the sample and the reference probe pulses were spectrally dispersed in a home-build prism spectrograph assembled by Entwicklungsbüro Stresing, Berlin and detected separately, shot-to-shot, by a pair of charge-coupled devices (CCD detectors, Hamamatsu S07030-0906).

TA spectra analysis.

The absorption change upon pumping at 600 nm (i.e. slightly higher in energy than the direct excitonic states in MoS_2) was probed at different time delays after photoexcitation. The resulting absorption change spectra for -0.2 ps ~1 ns after pump excitation are shown for MoS_2 bare films in Figure S13, while the global analysis results are demonstrated in Figure S14.

Similar to the previous report,[S4] negative TA bands observed at short delay time (< 1 ps) at 611 nm and 674 nm are attributed to the photobleaching (PB) from the excitonic states B and A, respectively. The pulse width limited rise time observed for the excitonic transitions implies that the photogenerated species dissipate excess kinetic energy faster than ~ 80 fs (temporal resolution of the experiment). The excitonic PB peaks decay rapidly in less than 10 ps and blue-shifted to 589 nm and 647 nm for A and B transitions, respectively (see long-time spectrum in Figure S14). We attribute these higher-energy PB bands to the presence of free charge carriers at the direct band edges. The energy difference between the negative peaks from the excitonic states and the free carriers gives the exciton binding energy, which is found to be ca. 80 meV for the few-layer 2D MoS_2 nanoflakes used in this work (for reference, in MoS_2 the exciton binding energy in the bulk material is ca. 40 meV and increases to up to ca. 900 meV in the monolayer[S5, S6]). We note that due to photoinduced absorption (PIA) effects, the presence of free carriers at the direct band edges at long times also results in positive TA signals, which coincide with the wavelengths of the excitonic transitions, so the overall TA spectrum of the free charges resembles the mirror image of the exciton spectrum. Moreover, fluence-dependent studies inducate that the long-lived (> 1 ns) free charge carriers are predominantly generated on the sub-100 fs time scale, rather than by slower dissociation of the excitons which recombine within a few ps.

Compared to the bare MoS_2 film, the TA spectra of the MoS_2/DHA-PDI film have identical features at all time delays (Figure S14), which indicates that the TA signatures of the DHA-PDI do not interfere with signals from the MoS_2. Indeed, due to the negligible absorption at the pump wavelength and the thinness of the DHA-PDI layer, the organic layer shows TA signals with intensity two orders of magnitude lower compared to MoS_2 flakes (see Figure S15 for a film containing only 10 nm DHA-PDI). Moreover, we note that the TA of both MoS_2 and MoS_2/HDA-PDI films was measured with similar pump fluence (~ 1 µJ cm^{-2}), which ensures a similar number

of absorbed photons and initial excitations in both cases. Compared to bare MoS_2, the TA spectra of the MoS_2/DHA-PDI film show a smaller amplitude of the excitonic states signals recorded at early time delays $t = 0.1$ ps (see Figure 3c in main text), while a higher amplitude of the charge signature is observed at long-time, which is consistent with the global analysis results shown in Figure S14 and the normalized temporal evolution of signals at 611 nm and 674 nm (Figure 3d in the main text). We note that the TA signals at early times is dominated by the excitons, however, could be affected by the signal from free charge due to the fast charge generation[S4] and the wavelength overlapping of the TA signals, i.e. PB for exciton and PIA for free charges. Therefore, the smaller initial signal for the hybrid film could also be attributed to the higher free charge compared to the MoS_2 bare film. To confirm the increased presence of long-lived free carriers at the direct band edges in the hybrid films compared to the bare MoS_2, TA measurements with different initial carrier densities were carried out by increasing the excitation fluence to 2 µJ /cm^2 (see Figure S16). An identical relative behavior of the temporal evolution for the free charges and the excitonic transitions was observed. We also note that using higher energy pump photons (3 eV) gave similar trends.
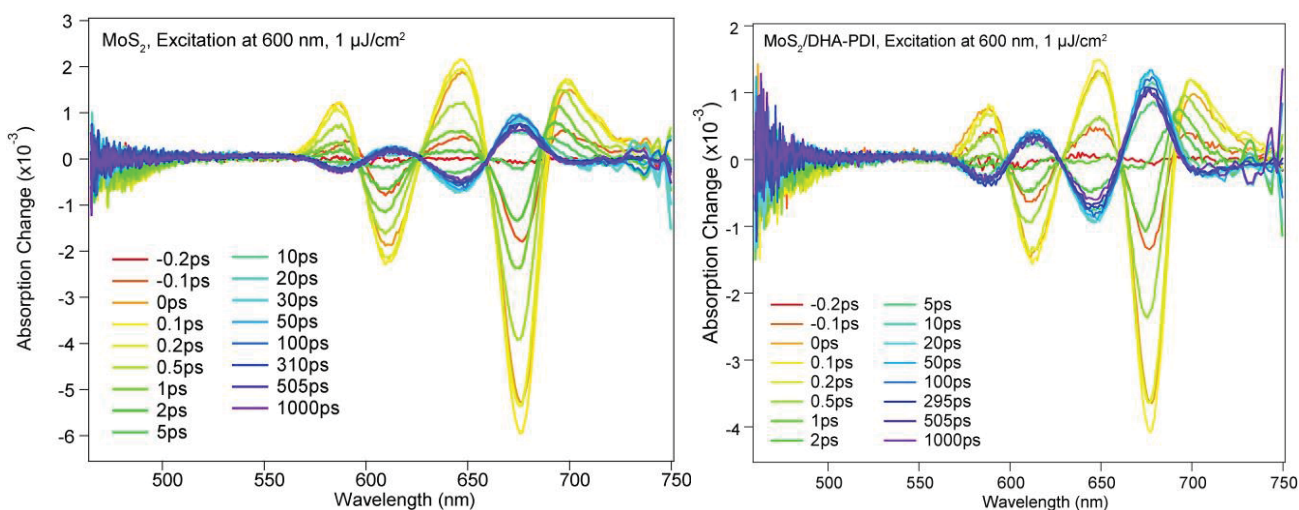

Figure S13. TA spectra of MoS_2 (left) and MoS_2/DHA-PDI (right) at different time decays using excitation at 600 nm and a pump fluence of ca. 1 µJ cm^{-2}.
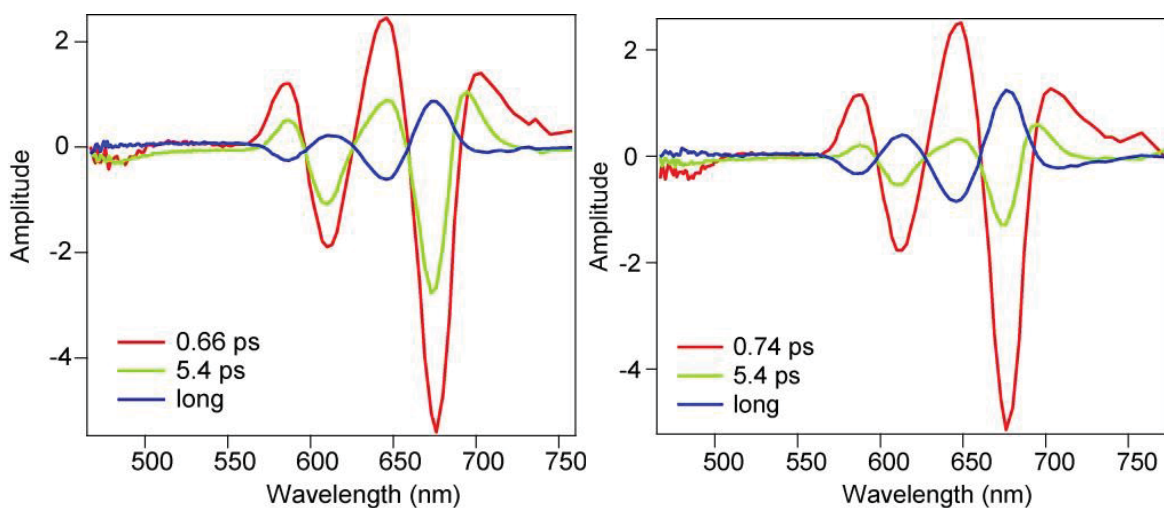
Figure S14. Amplitude spectra for MoS_2 (left) and MoS_2/DHA-PDI (right) from three-exponential global analysis of the TA spectra shown in Figure S13.
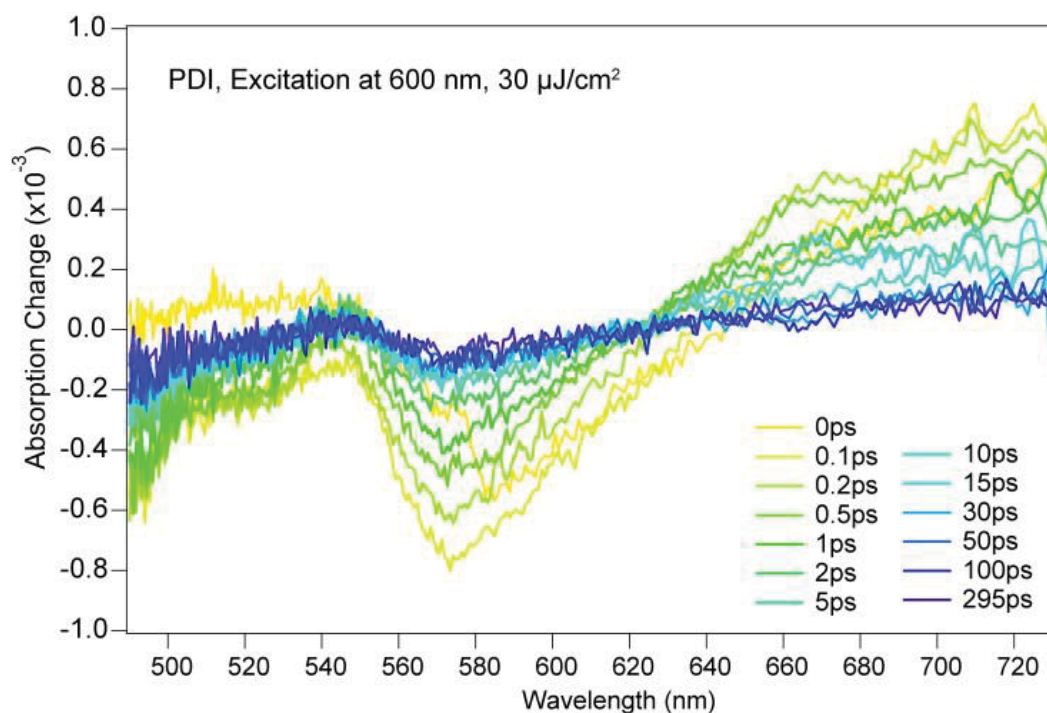

Figure S15. Transient absorption spectra of a 10 nm DHA-PDI thin film with excitation of 600 nm. The incident pump fluence is 30 μJ/cm^2, which is 30 times higher than the fluence used for MoS_2 or MoS_2/DHA-PDI film measurements.
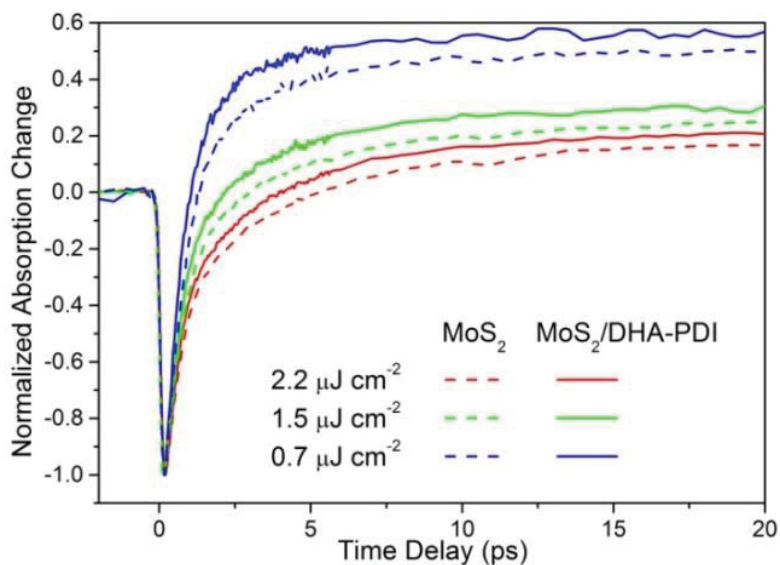
Figure S16. Normalized temporal evolution of the absorption change under different pump fluence conditions. The curves are plotted for probe photon energies in resonance with the excitonic A transition using excitation λ_{pump} = 600 nm.

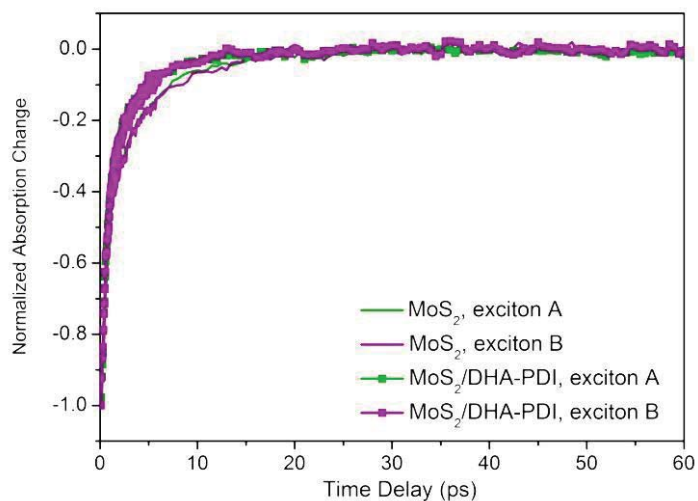**Figure S17**. Normalized absorption change at A and B excitonic resonances for MoS_2 and hybrid MoS_2/DHA-PDI films after subtracting the positive signal due to the presence of free charges.

References.

S1) Yu, X.; Prevot, M. S.; Guijarro, N.; Sivula, K., Self-assembled 2D WSe2 thin films for photoelectrochemical hydrogen production. *Nat. Commun.* **2015,** *6*, 7596.

S2) Rehm, S.; Stepanenko, V.; Zhang, X.; Rehm, T. H.; Würthner, F., Spermine-Functionalized Perylene Bisimide Dyes—Highly Fluorescent Bola-Amphiphiles in Water. *Chemistry – A European Journal* **2010,** *16*, 3372-3382.

S3) Savage, R. C.; Orgiu, E.; Mativetsky, J. M.; Pisula, W.; Schnitzler, T.; Eversloh, C. L.; Li, C.; Mullen, K.; Samori, P., Charge transport in fibre-based perylene-diimide transistors: effect of the alkyl substitution and processing technique. *Nanoscale* **2012,** *4*, 2387-2393.

S4) Tsokkou, D.; Yu, X.; Sivula, K.; Banerji, N. The Role of Excitons and Free Charges in the Excited-State Dynamics of Solution-Processed Few-Layer MoS_2 Nanoflakes. *J. Phys. Chem. C* **2016**, *120*, 23286-23292.

S5) Komsa, H.-P.; Krasheninnikov, A. V. Effects of confinement and environment on the electronic structure and exciton binding energy of MoS_2 from first principles. *Phys. Rev. B* **2012**, *86*, 241201.

S6) Hill, H. M.; Rigosi, A. F.; Roquelet, C.; Chernikov, A.; Berkelbach, T. C.; Reichman, D. R.; Hybertsen, M. S.; Brus, L. E.; Heinz, T. F. Observation of excitonic Rydberg states in monolayer MoS_2 and WS_2 by photoluminescence excitation spectroscopy. *Nano Lett.* **2015**, *15*, 2992-2997.